This is a postprint of: Microporous and Mesoporous Materials 109 (2008) 525-534

EFFECT OF THE SiO_2/Na_2O RATIO ON THE ALKALI ACTIVATION OF FLY ASH. PART II: ^{29}Si MAS-NMR SURVEY

M. Criado, A. Fernández-Jiménez, A. Palomo, I. Sobrados and J. Sanz

Eduardo Torroja Institute (CSIC), c/ Serrano Galvache, nº4, 28033, Madrid, Spain

Instituto Ciencia de Materiales (CSIC), Cantoblanco, 28049 Madrid, Spain

Abstract

^{29}Si MAS-NMR spectroscopy was used to characterize the reaction products resulting from the alkali activation of a type F fly ash. Specifically, analyses focused on the degree of polymerization of the activating solution (SiO_2/Na_2O ratio = 0.0, 0.19, 0.69 and 1.17) and thermal curing time (from 8 h to 180 days at 85 ºC). The results obtained showed that the nature of the alkali activator plays an important role in the kinetics, structure and composition of the gel initially formed. The alkaline aluminosilicate gel formed exhibits short-range order, with the silicon appearing in a wide variety of $Q^4(nAl)$ (n=0, 1, 2, 3 and 4) environments. In the absence of soluble silica (SiO_2/Na_2O ratio = 0.0, 0.19), the Al-rich gels initially generated evolved rapidly into zeolites. At higher levels of anion polymerization (SiO_2/Na_2O ratio ≥ 0.5), zeolite crystallization was retarded.

Keywords: Fly ash, ^{29}Si MAS-NMR, silicate-sodium oxide ratio

1. Introduction

The alkali activation of fly ash (AAFA) is a unique procedure in which the greyish-black powdery ash (FA) is mixed with alkaline activators (alkaline solutions) and then cured at a certain temperature to form aluminosilicate materials. In this process, glassy constituents of the fly ash are transformed into a compact cement **[1-5].** Previous studies **[6-9]** have shown that the primary reaction product formed in AAFA is an X-ray amorphous aluminosilicate gel (N-A-S-H) containing silicon and aluminium tetrahedra randomly distributed in tetrahedral networks. The cavities formed in these gels when the networks are cross-linked can accommodate alkaline cations that offset the electrical charge generated due to Si^{4+} replacement by Al^{3+} ions **[1-3]**. Moreover, the short-range structural order exhibited by the nano-crystalline materials that appear in a subsequent stage improves the mechanical properties of the hardened pastes. In some cases several types of zeolites (hydroxysodalite, Na-chabazite, zeolite Y, and so on) also form as secondary reaction products **[7-10]**).

Prior papers stressed the importance of the characteristics of the prime materials ("*reactive*" aluminium plays a key role in the kinetics of aluminosilicate gel formation **[8]**), the curing conditions (time and temperature) **[3,4,11-13]** and the nature and concentration of the alkali activator used **[10,14]**. In addition, the presence of soluble silica is known to improve the mechanical properties of the resulting material **[4-6]** at early ages. Palomo et al. found that after curing at 85 ºC for 24 hours, different types of fly ash activated with 8-12M NaOH yielded a material with mechanical strength ranging from 35 to 40 MPa, and up to 90 MPa when waterglass was added to the NaOH solution (SiO_2/Na_2O=1.23). The addition of a small amount of monomeric soluble silica was observed to spur the activation reactions. The inclusion of more than 2% soluble silica modifies reaction kinetics substantially. The presence of soluble silica also affects the rate of crystallization and the type of zeolites formed

as secondary reaction products ((D6R-type) herschelite; zeolite Y; (S4R-type) zeolite P) **[9,10]**.

In light of the difficulties encountered in the XRD characterization of alkaline aluminosilicate gel reaction products (zeolite precursors), conscientious efforts have been made in recent years to interpret the information furnished by other analytical techniques **[3,8-13]**. In one previous study **[10]** using infrared spectroscopy, for instance, the gel was found to comprise primarily bridge and terminal Si-O bonds. Earlier papers **[6-8,11]** described the advantages of NMR techniques for characterizing three dimensional short-range ordered materials in which silicon is found in a variety of environments, predominantly Q^4(nAl) (n=0, 1, 2, 3 and 4).

The present study aimed to establish a correlation between the presence of soluble silica in the activating solution and the nature and composition of the reaction products formed (N-A-S-H gel and zeolites) as well as reaction kinetics. Three solutions with different SiO_2/Na_2O ratios and an 8M NaOH control solution were used to activate the fly ash. ^{29}Si MAS-NMR spectroscopy was used **[10]** in this study to reach a clearer understanding of the mechanisms controlling the activation processes involved and their respective kinetics.

2. Experimental

2.1 Materials

A class F (ASTM C 618-03) fly ash from the steam power plant at Compostilla, Spain was used in the present study. The chemical composition of the initial ash is given in Table 1 and a much more exhaustive characterization in a previous paper **[7]**.

Table 1.- Chemical analysis of the initial fly ash (%)

The ash was activated with a series of alkaline solutions, all with practically constant sodium oxide content but varying proportions of soluble silica. The products used to prepare the solutions were laboratory reagents: ACS-ISO 98% NaOH pellets supplied by Panreac S.A. and sodium silicate (density of 1.38 g/cc) with composition: 8.2% Na_2O, 27% SiO_2 and 64.8% H_2O supplied by Manuel Riesgo S.A. Adding different amounts of sodium silicate to the reaction medium varied the total silica content of the solutions. The composition of the working solutions is shown in Table 2.

Table 2. Chemical composition of the working solutions, by mass

The pastes were prepared by mixing the fly ash with activating solutions, using a liquid/solid ratio of 0.4, by mass. The pastes were cured in an oven at 85 ºC for 8 hours and 7, 28, 90 and 180 days. The nominal Si/Al composition of the pastes prepared was 1.89, 1.93, 2.02, and 2.10 when the fly ash was activated with solutions N, W15, W50 and W84.

2.2 Techniques

^{29}Si MAS-NMR (Avance-400 Bruker apparatus) analyses were conducted on the initial fly ash, the alkaline solutions and the pastes formed at the various reaction times. The ^{29}Si resonance frequency was 79.5 MHz and the spinning rate 10 kHz. Spectra were obtained after irradiation of the sample with a $\pi/2$ pulse (5μs). The time between accumulations was 5s. All measurements were taken at room temperature with TMS (tetramethylsilane) as the external

standard. The error in chemical shift values was estimated to be lower than 0.5 ppm. Samples were exposed to a strong magnetic field prior to characterization to lower the iron content and thereby reduce paramagnetism-induced distortions in NMR spectra. The crystalline phases forming during fly ash activation were identified with XRD (Philips PW-1730).

3. Results

Although the primary aim of this study was to acquire an understanding of the nanostructure of the aluminosilicate gel formed as a result of the alkali activation of fly ash, exploration of this question was preceded by the characterization of the prime materials used (ash and alkaline solutions).

3.1 Prime materials

Figure 1 shows the spectrum for the initial ash. Its very wide and poorly defined profile is indicative of the heterogeneous distribution of the silicon atoms in this material. Deconvolution of the NMR spectra revealed the presence of eight components **[7]**. The peaks detected at ≈ -80, -84, -94, -100, -104 and –108 ± 1 ppm were associated with the initial vitreous material **[7,15]**. The peak at -90 ppm was attributed primarily to the Q^3(3Al) Si units in the mullite present in the fly ash **[16]**, while most of the peaks appearing above -108 ppm were assigned to different crystalline phases of silica (Q^4(0Al) signals) **[17]**. The results of deconvoluting the initial ash spectrum, assuming constant bandwidth, are listed in Table 3.

Figure 1. ^{29}Si MAS-NMR spectrum of the initial fly ash

Table 3. Deconvolution of the ^{29}Si MAS-NMR spectrum of the initial fly ash

Figure 2 shows the ^{29}Si MAS-NMR spectra of the three solutions containing soluble silica used in the study (W15, W50 and W84). The solution ***W15*** spectrum exhibited a single peak at -70.7 ppm, associated with the presence of Q^0 units (monomers) **[17]**. The solution ***W50*** spectrum had three peaks, one more intense at -71 ppm and the other two at -78.6 ppm and -80.7 ppm; these signals were respectively assigned to Q^0, Q^1 (dimer) and Q_{cy}^2 (cyclic trimer) units **[17]**. The six peaks observed on the solution ***W84*** spectrum, at positions -70.8, -78.4, -81.0, -86.3, -88.6 and -94.3 ppm, are indicative of a more intense polymerization of the Si tetrahedra. In the literature of sodium silicates **[17-21]**, these signals are attributed to the presence of monomers, dimers, linear trimers and bridged cyclic tetramers, see Figure 2(b) **[17].** These data show that for similar concentrations of Na_2O (see Table 2), the increase on the silicate ion concentration induce a greater polymerization of the silicate units in the solution **[17]**.

Figure 2. (a) ^{29}Si MAS-NMR spectra of the alkaline solutions used; (b) ^{29}Si chemical shift, δ, of the silicate anion in silicate solutions, identified in accordance with the literature **[17,18]**.

3.2 Alkali-activated fly ash pastes

The pastes obtained at different thermal curing ages were XRD-characterized prior to NMR analysis. Although the XRD results are not described here, some of the findings are shown in Figure 3.

Figure 3. X-ray powder diffraction patterns of ash activated with different alkaline solutions (28 and 180 days).

Generally speaking, the main reaction product was a sodium aluminosilicate gel, from which certain zeolites may form as secondary products. This aluminosilicate gel can be regarded to be a zeolite precursor **[8,22].** The type and amount of zeolites found varied with the nature of the alkaline activator and thermal curing time.

In pastes activated with solutions ***N*** and ***W15***, for instance, hydroxysodalite and Na-chabazite were detected at a reaction time of 8 hours. The amount of Na-chabazite increased with curing time and was slightly higher in the materials generated when the ash was activated with solution ***W15*** (9.9% after 8 hours and 36.8% after 180 days (see Figure 3A) **[22]**).

In samples activated with the ***W50*** solution, however, zeolites were not detected until the 28th day of thermal treatment (5.7% zeolite Y, see Figure 3B) **[22]**). Zeolite Y was observed to gradually evolve into phillipsite (8.3% zeolite Y after 90 and 10.1% phillipsite after 180 days). Small amounts of Na-chabazite were also detected (2.3%) at 180 days (see Figure 3B) **[22]**). Finally, the amount of zeolites detected was lower in the products generated when solution ***W84*** was used as the activator: zeolite P was detected only after 28 days (increasing from 1.1% to 6.7% at 180 days (see Figure 3B) **[22]**). Small amounts of phillipsite (0.7% at 28 days and 4.4% at 180 days, see Figure 3B) were also observed to form in these samples **[22]**.

The ^{29}Si NMR spectra of fly ash activated with the different alkaline solutions are shown in Figures 4 and 5. The changes detected in these spectra reveal chemical transformations taking place during alkali activation of the initial fly ash. The experimental profiles were deconvoluted with WIN NMR 1D software, using the assignments reported in previous

studies **[8,11,17,18]**. In the present analysis, a constant bandwidth was assumed for all components. The results obtained are described in Figures 4 and 5

Figure 4. ^{29}Si MAS NMR-MAS spectra of AAFA pastes activated with solution (a) N and (b) W15.

After 8 hours of reaction time, the spectra obtained for the pastes activated with solutions ***N*** and ***W15***, shown in Figure 4(a) and (b), exhibited peaks at -84, -88, -93, -99, -104 and -108 ± 1 ppm, i.e., signals located in approximately the same positions as the spectra of certain zeolites (see Table 4) **[17,18,23-25].** The area of the signal at -84 ppm, assigned to hydroxysodalite-type Q^4(4Al) units **[23]** (phase detected in XRD analysis, see Figure 3A **[22]**), remained practically unchanged throughout the activation process. The signals appearing at -88, -93, -99, -104 and –108 ppm, were attributed to silicon tetrahedra surrounded, respectively, by Al_4, $SiAl_3$, Si_2Al_2, Si_3Al_1 and Si_4 **[17,18,24,25]** (see Table 5) in the Na-chabazite structure **[17-18]**. The signals appearing at values higher than -108 ppm were associated with Q^4(0Al) units, i.e., silica polymorphs **[17]** such as quartz (-108 ppm), coesite (-108, -113.9 ppm) or cristobalite (-108 ppm).

The growing intensity of the Q^4(1Al) and Q^4(2Al) components with curing time (7, 28, 90 and 180 days) is indicative of the progressive increase in the amount of silicon units incorporated into the tectosilicate formed. The similarity between the spectra found for ***N*** and ***W15*** pastes suggests that the addition of a small amount of monomeric soluble silica in the system has no effect on the nature or composition of the reaction products. For short reaction times (8 hours of thermal curing) however, peak resolution was better in ***W15*** than in ***N*** spectra.

Table 4. ^{29}Si chemical shifts in zeolites (standard data)

Table 5. ^{29}Si NMR signals

Figure 5. ^{29}Si MAS NMR-MAS spectra of AAFA pastes activated with solution (a) W50 and (b) W84.

In the ***W50*** and ***W84*** spectra (ash activated with W50 and W84 solution; $SiO_2/Na_2O > 0.5$), shown in Figure 5(a) and (b), resolution was lower and the profile wider, suggesting that the silicon was surrounded by a wider range of environments; in other words, the degree of disorder was greater in this tectosilicate than in the preceding cases. These spectra showed practically no well-defined peaks until after 180 days of thermal treatment.

The centre of gravity of the eight-hour to ninety-day in W50 samples was about 5 ppm less negative than in the 180-day samples. XRD analysis showed that the zeolite initially forming in these samples was zeolite Y **[17,18,28]** with ^{29}Si NMR-MAS signals at -84, -87, -93, -100, and -106 ppm, attributed to silicon tetraedra surrounded, respectively, by Al_4, $SiAl_3$, Si_2Al_2, Si_3Al_1 and Si_4. The maximum intensity band on the 180-day spectrum was centred over -99 ppm, a finding indicative of the depletion of zeolite Y and the appearance of phillipsite (Figure 3B) corroborated by XRD. This would explain the shift in all the bands toward more negative values: -89.1,-93.4, -98.6, -103.6 y -108.6 (see Table 5, Figure 5B).

As in the samples activated with solutions ***N*** and ***W15***, the centre of gravity on the ***W84*** spectra was also recorded at -99 ppm. The deconvolution of these spectra again showed a

series of peaks at –89, -94, -98, -104 and –108 ± 1 ppm, allocated to environments in which the Si is surrounded by 4, 3, 2, 1, and 0 Al, respectively (see Table 5).

In all the samples analyzed, the signals appearing on W50 and W84 spectra at values lower than –80 ppm were associated with less condensed, residual species **[17,18]** and the peaks at values higher than –108 ppm with the $Q^4(0Al)$ environments found in quartz and cristobalite **[17,18]**.

4. Discussion

The alkali activation of fly ash is a staged process **[7,8,29]**. In the initial or ***dissolution*** stage, the fly ash comes into contact with the alkaline solution. The OH^- ions present in the reaction medium sever the Si-O-Si, Si-O-Al and Al-O-Al covalent bonds of the vitreous fly ash. Previous studies showed that aluminium initially dissolves at a faster rate than silicon. As the process continues, Si and Al are leached out of the ash stoichiometrically; and when the Al is depleted the rate of silica dissolution declines **[30-32]**.

The silicon and aluminium ions released into the medium form Si-OH and Al-OH groups. In the second, ***gel formation*** stage, the ionic species present in the solution (silicate and aluminate ions) condense to form Si-O-Al and Si-O-Si bonds, giving rise to an aluminosilicate gel. This product is characterized by a three-dimensional structure whose cavities house alkaline cations that offset the charge imbalance.

In the absence of soluble silicates in the activating solution, the stage believed to govern kinetics is the dissolution of the Al and Si released by the fly ash. Since Al-O bonds are more

readily broken than Si-O bonds, the Al concentration in the reaction medium rises in the early phases of the reaction. The Al and Si tetrahedra have time to organize before precipitating, giving rise to the formation of more orderly aluminosilicate gels. Well-defined ^{29}Si MAS-NMR spectra are then obtained and a high degree of zeolitization is observed at the earliest reaction times (8 hours **[8]**).

Given that the Si/Al ratios less than 1 are not possible (Loewenstein's rule) even where there is an excess of Al, the result of activation is a relatively scantly condensed aluminosilicate with a profusion of silicon in Q^4(4Al) units (see Figure 4(a), material **N**). This would partially explain the presence of hydroxysodalite with an Si/Al ratio of 1 after eight hours. The rest of the material subsequently dissolves and both Al and Si migrate from the ash to the medium. The gel then gains in silica content and in the amount of Q^4(2Al) and Q^4(1Al) units. Figure 6 compares the variation in intensity of the aluminium-rich structural units (Q^4(4Al)+Q^4(3Al)) to the variation in the silicon-rich units (Q^4(2Al)+Q^4(1Al)).

The NMR spectra of the system N show a centre of gravity at around -99 ppm (see Figure 4). A comparison of these spectra with zeolite profiles reveals similarities with spectra reported for Na-chabazite **[8,11,17,18,24,25,33]** (zeolite detected by XRD, see Figure 3A). Si/Al ratios were determined by applying Engelhard's equation **[17]** and assuming that the Loewenstein rule holds. In N-type pastes the Si/Al value is about 1.87, very close to the nominal ratio (1.89) as shown in Figure 7.

In systems ***W15***, ***W50*** and ***W84***, the presence of soluble silica in the medium, provided by the activator, would be expected to affect both the dissolution process and the nature of the chemical species initially forming. From the outset, when the aluminium released reacts with

the silicon ions in the solution, it forms compounds whose Si/Al ratios are ≥1. Higher concentrations of chemical species in the medium should shorten the time needed to induce gel formation. However, this assertion is not entirely accurate, because the gel formation kinetics is also partially conditioned by the amount and type of polymeric species (monomers, dimers and so on) present in the reactional medium.

In the alkaline solutions studied, the degree of polymerization varied significantly with the SiO_2/Na_2O ratio (see Figure 2). These results concur with findings previously reported **[17-21]**, according to which mean silicate ion connectivity depends on the SiO_2/Na_2O ratio and to a lesser extent on silica concentration. The fraction of Si in the form of Q^0 and Q^1 units declines with increasing SiO_2/Na_2O ratios, while the Q^2_{cycle} unit content grows. In other words, the degree of silicate ion polymerization in the alkaline solutions climbs with the rise in the silica/cation ratio or silica concentration **[17-21]**.

In systems activated with solution W15 (1.62% soluble silica, 100% monomer), the monomeric soluble silicates (Q^0 units) in solution readily react with the aluminate anions $(Al(OH)_4)^-$ released during fly ash dissolution, resulting in the fairly rapid formation of an initial alkaline aluminosilicate gel (Si/Al ratio = 1). These more labile, less stable species allow for a higher degree of structural organization and densification of the gel prior to hardening. High resolution spectra are obtained from eight hours onward, with the percentage of $Q^4(2Al)+Q^4(1Al)$ units consistently larger than the percentage of $Q^4(4Al)+Q^4(3Al)$ units (see Figure 6). In this case, as in the case of the materials activated with solution N, the centre of gravity is located at around -99 ppm. As the reaction progresses, the Si content in this gel rises, eventually raising the Si/Al ratio (1.88) to a value very close to the nominal 1.98 (see Figure 7). However the most significant difference between systems N and W15 is the slight

shortening of the polymerization-crystallization stage. Kinetically speaking, this process is more effective in system ***W15*** than in system ***N*** (which contains no additional soluble silicates).

System W50, soluble silica content = 5.40%, 85% of which in monomeric or dimeric form; spectral patterns are less sharply defined than in the preceding systems due to the higher degree of polymerization. The centre of gravity of the spectrum is observed to shift to values 5 ppm less negative, even in eight-hour to ninety-day samples. According to the literature **[34-35]**, dimers can react more rapidly than monomers with the Al from the fly ash solution; this, in conjunction with the higher concentration of Si, gives rise to the formation of initially metastable gels with Si/Al ratios > 2. The formation of such Si-rich gels explains why it takes more time for zeolites with Si/Al ratios ≥ 2 (zeolite Y-type) to crystallize. Gel metastability is the outcome of the shift in the centre of gravity taking place between 90 hours and 180 days, produced by the transformation of zeolite Y into phillipsite (Oswald's rule, **[36-38]**) see Figure 8 **[22]**.

Figure 6 shows that the percentage of silica-rich units is much higher than the percentage of alumina-rich units. Nonetheless, as the reaction progresses and the amount of Al and Si released by the ash increases, the system evolves toward its most thermodynamically stable composition, with 180-day Si/Al ratios of 1.91, very similar to the nominal 2.02 and to the values obtained in other systems. That is to say, the formation of these units with such solutions is more a result of favourable kinetics than of thermodynamic stability.

System W84, soluble silica content = 9.07%; ≈ 50% in the form of cyclic trimers: in this case the addition of a larger amount of more highly polymerized silicates (see Figure 5) fails to

generate well defined spectra even at 90 days. Nonetheless, similarities can be observed between this system and systems N and W15 in terms of both the centre of gravity (around -99 ppm) and the Si/Al ratio, which increases with time, to 1.80 as 180 days as shown in Figure 7, slightly lower than the nominal ratio of 2.10.

According to the literature **[34,35]**, cyclic silicate trimers react relatively slowly with the Al from fly ash. The phases formed are nonetheless fairly stable, which may be what retards the subsequent reaction of the material. In addition, when more highly polymerized silica is added, the gel restructuring rate also declines **[30,34,35]**. The gel begins to harden while a substantial portion of the ash has yet to react and only small amounts of gel have formed **[22]**.

That would explain why lower initial reaction rates were observed in this case (the eight-hour reaction rate for ***W84*** was 35.47% and the seven-day rate was 39.18%, whereas the seven-day rates for ***W50***, ***W15*** and ***N*** were 51.58%, 54.44% and 51.30% respectively) and the compounds formed had a lower Si/Al ratio. The decline in the reaction rate can also be deduced from the results in Figure 6 where, despite an initially higher silica content in ***W84***, the compounds richer in silica did not form until the 28th day.

The findings of this study show that the Si/Al ratio should not be increased indefinitely. There appears to be a threshold value of around 2, the composition toward which different systems tends regardless of the initial conditions, possibly because it constitutes the most thermodynamically stable state. Similar results have been reported using fly ash with different Si/Al ratios **[4,8]**, or metakaolin **[30]**.

Conclusions

The primary reaction product of the alkali activation of fly ash is an amorphous gel consisting in a polymeric, cross-linked aluminosilicate network whose Si/Al ratio depends on curing time and the nature of the alkaline activator used.

The nature of the alkali activator plays an instrumental role in the kinetics, structure and composition of the gel initially formed. The addition of soluble silica affects the intermediate stages of the activation reaction but not the final result.

The present study shows that the degree of polymerization of the predominant silica species in the activating solutions used has the following effects: (1) monomers and dimers shorten the time needed to induce gel-formation reactions; (2) the presence of a higher percentage of dimers leads to the speedier formation of gels, which are, however, less thermodynamically stable; and (3) the presence of cyclic silicate trimers gives rise to initially more stable gels that retard the subsequent reaction of the ash.

Acknowledgements

Funding for this research was provided by the Directorate General of Scientific Research under project BIA2004-04835; a post-doctoral contract associated with the study was awarded by the CSIC and co-financed by the European social fund (REF. I3P-PC2004L).

References

[1] P.V. Krivenko, “Alkali cements” First International Conference of Alkaline Cements and Concretes, Ukraine, Kiev, (1994), 11-129.

[2] A. Palomo, M.W. Grutzeck, M.T. Blanco, 29, (1999), 1323-1329.

[3] P. Duxson, A. Fernández-Jiménez, J.L. Provis, G. C. Lukey, A. Palomo J. S. J. van Deventer, J. Materials Science (in press).

[4] A. Fernández-Jiménez , A. Palomo and C. López-Hombrados, ACI Materials Journal, 103 (2), (2006), 106-112.

[5] G. Kovalchuk, A. Fernández-Jiménez, A. Palomo, Mater Construc (in press).

[6] W.K.W. Lee, and J.S.J. Van Deventer, Colloids and Surfaces A: Physicochem. Eng. Aspects, 211, (2002), 49-66.

[7] A. Fernández-Jiménez, A. Palomo, Fuel, 82, (2003), 2259-2265.

[8] A. Fernández-Jiménez, A. Palomo, I. Sobrados, J. Sanz, Microp. Mesop. Mat., 91, (2006), 111-119.

[9] A. Fernández-Jiménez, A. Palomo, Microp. Mesop. Mat., 86, (2005), 207-214.

[10] M. Criado, A. Fernández-Jiménez and A. Palomo, Microp. Mesop. Mat. **(**Submitted for publication).

[11] A. Palomo, S. Alonso, A. Fernández-Jiménez, I. Sobrados, J. Sanz, J. Am. Ceram. Soc., 87, (2004), 1141-1145.

[12] J.S.J. van Deventer P. Duxson, G.C. Lukey, Langmuir, 22, (2006), 8750-8757.

[13] M. Criado, A. Palomo, A. Fernández-Jiménez, Fuel, 84, (2005), 2048-2054.

[14] A. Fernández-Jiménez, A. Palomo, Cem. Concr. Res., 35, (2005), 1984-1992.

[15] A. Fernández-Jiménez, A. G. de la Torre, A. Palomo, G. López-Olmo, M. M. Alonso, M. A. G. Aranda, 85, (2006), 625-634.

[16] S. Gomes, M. François, Cem. Concr. Res., 30, (2000), 175-181.

[17] G. Engelhardt, D. Michel “High Resolution Solid State NMR of silicates and zeolite”, Ed. Wiley, (1987), Londres. Inglaterra.

[18] J. Klinowski “Nuclear Magnetic Resonance Studies of Zeolites”, Progress in NMR Spectroscopy, 16, (1984), 237-309.

[19] G. Engelhardt, D. Zeigan, H. Jancke, W. Wieker, D. Hoebbel , Z. Anorg. Allg. Chem., 418, 1, (1975), 17-28.

[20] R. K. Harris, C. T. G. Knight, J. Molecular Structure, 78, (1982), 273-278.

[21] R. K. Harris, J. Jones, C. T. G. Knight, R. H. Newman, J. Molecular Liquids, 29, (1984), 63-74.

[22] M. Criado, A. Fernández-Jiménez, A. G. de la Torre, M. A. G. Aranda A. Palomo, Cem. Concr. Res. (available on line).

[23] G. Engelhardt, S. Luger, J.Ch. Buhl and J. Felsche, Zeolites, 9, (1989), 182-186.

[24] E. Lippmaa, M. Magi, A. Samoson, M. Tarmak and G. Engelhardt, J. Am. Chem. Soc., 103, (1981), 4992-4996.

[25] P.S. Neuhoff, J.F. Stebbins and D.K. Bird, American Mineralogist, 88, (2003), 410-423.

[26] A. Madani, A. Aznar, J. Sanz, J. M. Serratosa, J. Phys. Chem., 94, (1990), 760-765.

[27] M. Kato, H. Nishido, Microp. Mesop. Mat., 61, (2003), 261-371.

[28] X.S. Zhao, G.Q. Lu and H.Y. Zhu, J. of Porous Materials, 4, (1997), 245-251.

[29] A. Fernández-Jiménez, A. Palomo, M. Criado, Cem. Concr. Res., 35, (2005), 1204-1209.

[30] P. Duxson, J.L. Provis, G. C. Lukey, S. W. Mallicoat. W. M. Kriven, J.S.J. van Deventer, Colloids and surfaces A: Physicochem. Eng. Aspects, 269, (2005), 47-58.

[31] E. H. Oelkers and S. R. Gislason, Geochimica et Cosmochimica Acta, 65, (2001), 3671-3681.

[32] S.J. Kohler, F. Dufaud and E.H. Oelkers, Geochimica et Cosmochimica Acta, 67, (2003), 3583-3594.

[33] A. Dyer "An introduction to zeolite molecular sieves", Ed. Wiley, (1988), New York, USA.

[34] M.R. Anseau, J.P. Leung, N. Sahai, and T.W. Swaddle, Inor. Chem, 44, (2005), 8023-8032.

[35] R.K. Iler, "The chemistry of silica" Ed. Wiley, New York (1979)

[36] R. Barrer "Hydrothermal Chemistry of Zeolites", Ed. Academic Press, (1982), England.

[37] T. Threlfall, Organic Process Research & Development, 7, (2003), 1017-1027.

[38] D.W. Breck "Zeolita Molecular Sieves", Ed. Krieger, (1974), Florida, USA.

Tables

Table 1.-. Chemical analysis of the initial fly ash (%)

Table 2. Chemical composition of the working solutions, by mass

Table 3. Deconvolution of the ^{29}Si MAS-NMR fly ash spectrum

Table 4. ^{29}Si chemical shifts in zeolites (standard data)

Table 5. ^{29}Si NMR signals

Figures

Figure 1. ^{29}Si MAS-NMR of the initial fly ash

Figure 2. (a) ^{29}Si MAS-NMR spectra of the alkaline solutions used; (b) ^{29}Si chemical shift, δ, of the silicate anion in silicate solutions, identified in accordance with the literature **[17,18]**.

Figure 3. X-ray powder diffraction patterns of ash activated with different alkaline solutions (28 and 180 days).

Figure 4. ^{29}Si MAS NMR-MAS spectra of AAFA pastes activated with solution (a) N and (b) W15;

Figure 5. ^{29}Si MAS NMR-MAS spectra of AAFA pastes activated with solution (a) W50 and (b) W84

Figure 6. Variation in aluminium-rich ($Q^4(4Al)+Q^4(3Al)$) and silicon-rich ($Q^4(2Al)+Q^4(1Al)$) environments with reaction time, deduced from the ^{29}Si MAS NMR spectra for alkali-activated fly ash materials

Figure 7. Si/Al ratios versus time in fly ash activated with solutions: N; W15; W50 and W84

Figure 8. Percentage of zeolite phases in the matrices studied vs curing time (data obtained with XRD, using Rietveld methodology **[22]**).

Table 1.-. Chemical analysis of the initial fly ash (%)

L.I.(%)	I.R.	SiO_2	Al_2O_3	Fe_2O_3	CaO	MgO	SO_3	K_2O	Na_2O	TiO_2	Total
3.59	0.32	53.09	24.80	8.01	2.44	1.94	0.23	3.78	0.73	1.07	100

L.I. = loss on ignition; I.R. = insoluble residue

Table 2. Chemical composition of the working solutions, by mass

SOLUTION	OXIDE COMPOSITION (%)			SiO_2/Na_2O MODULUS
	Na_2O	SiO_2	H_2O	
N	7.81	0	92.19	-
W15	8.41	1.62	89.97	0.19
W50	7.84	5.40	86.76	0.69
W84	7.72	9.07	82.21	1.17

Table 3. Deconvolution of the ^{29}Si MAS-NMR fly ash spectrum

Pos. (ppm)	***-80.1***	***-84.5***	***-90.8***	***-95.2***	***-99.8***	***-104.3***	***-109.1***	***-114.5***	***120.4***
Width	5.21	5.21	5.21	5.21	5.21	5.21	5.21	5.21	5.51
Integral (%)	2.90	4.56	9.04	11.64	17.80	17.00	19.93	10.50	6.63

Table 4. ^{29}Si chemical shifts in zeolites (standard data)

Zeolite	**unit cell composition**	**Symbol**	**(Si/Al) NMR**	**^{29}Si chemical shifts (ppm from TMS)**					**Ref**
				Si(4Al)	**Si(3Al)**	**Si(2Al)**	**Si(1Al)**	**Si(0Al)**	
Hydroxysodalite	**$Na_8[SiAlO_4]_6(OH)_2.4H_2O$**	**HS**	**1.0**	**-84.5**					**[23]**
Ca chabazite	**$Ca_5Al_{10}Si_{26}O_{27}.40H_2O$**	**Cb-Ca**	**2.6**		**-94.0**	**-99.4[a]**	**-104.8**	**-110.0**	**[17,18]**
	$Ca_2[(AlO_2)_4(SiO_2)_8]13H_2O$	**Cb-Ca**	**2.0**		**-94.0**	**-99.4[a]**	**-104.8**	**-110**	**[24]**
Na chabazite	**$NaAlSi_2O_6.3H_2O$, Si/Al= 2**	**Cb-Na**	**1.84**	**-88.6**	**-93.2**	**-98.5[a]**	**-104.2**	**-109.7**	**[25]**
Na phillipsite	**$Na_{0.9}Ca_{0.5}K_{0.6}Si_{5.2}Al_{2.8}O_{16}.6(H_2O)$**	**Pt**	**1.9**	**-87.5**	**-92.0**	**-98.0[a]**	**-103.5**	**-108.0**	**[26,27]**
NaP zeolite	**$Na_2Al_3Si_5O_{16}.6H_2O$**	**P**	**1.6/ 1.9**	**-88**	**-92**	**-97**	**-102**	**-107**	**[17]**
Faujasite		**F**	**2.0**	**-84.0**	**-88.6**	**-93.7**	**-98.6**	**-104.6**	**[17,19]**
NaY zeolite	**$Na_{1.88}Al_2Si_{4.8}O_{13.54}\,9H_2O$**	**Na-Y**	**2.0/ 2.4**	**-83.8**	**-89.2**	**-94.5[a]**	**-100.0**	**-105.5**	**[17,18, 28]**

[a] *Highest intensity peak*

Table 5. ^{29}Si NMR signals

Sample		Residual xylanol group		Aluminosilicate gel					[b]$Q^4{}_x$	[c]Ref. zeolite	[d](Si/Al) NMR
			Si(4Al)	Si(4Al)	Si(3Al)	Si(2Al)	Si(1Al)	Si(0Al)			
N	**8h**		-82.4	-88.2	-93.2	-98.5[a]	-103.5	-109.2	-118.9	Sod,Cb	1.85
	7d		-83.9	-88.2	-93.3	-98.9[a]	-104.0	-108.8	-115.1	Sod,Cb	1.83
	28d		-84.5	-88.3	-93.3	-98.7[a]	-104.0	-180.4		Sod,Cb	1.78
	90d	-79.4	-83.2	-89.3	-93.3	-98.6[a]	-104.0	-108.7		Sod,Cb	1.83
				-86.9[e]							
	180d		-83.6	-88.5	-93.5	-98.9[a]	-104.1	-109.0	-115.9	Sod,Cb	1.87
W15	**8h**	-81.5		-87.9	-93.2	-98.7[a]	-103.9	-108.8	-114.2	Sod,Cb	1.76
	7d		-84.3	-88.2	-93.3	-98.7[a]	-104.3	-108.8	113.6	Sod,Cb	1.81
	28d		-84.9	-88.7	-93.5	-98.8[a]	-104.1	-108.7	-112.4	Sod,Cb	1.82
	90d		-84.5	-88.5	-93.4	-98.7[a]	-104.1	-109.4		Sod,Cb	1.81
	180d		-84.6	-88.7	-93.5	-98.7[a]	-104.0	-108.0	-111.4	Sod,Cb	1.88
W50	**8h**	-72.2	-80.0	-	-87.3	-93.7[a]	-100	-107.6	-115.1	-	2.02
	7d	-73.7	-81.7	-	-87.9	-94.0[a]	-100.1	-106.8	-113.6	-	2.04
	28d		-78.9	-84.5	-89.2	-94.4[a]	-100.4	-106.8	-113.6	Y	1.95
	90d		-78.9	-84.5	-89.2	-94.4[a]	-100.4	-106.8	-113.5	Y	1.95
	180d	-80.7	-85.1	-89.1	-93.4	-98.6[a]	-103.6	-108.6	-113.2	Pt	1.91
W84	**8h**	-81.3	-85.5	-89.1	-93.7	-98.4	-103.1	-108.1	-114.2	-	1.82
	7d	-80.6	-85.2	-89.3	-94.2	-99.6	-105.8	-111.1	-117.3	-	1.74
	28d	-74.5	-81.9	-87.2	-92.7	-97.9	-103.2	-109.3	-116.5	P	1.78
	90d	-80.6	-85.2	-89.3	-93.4	-98.1[a]	-103.4	-108.0		P, Pt	1.77
	180d		-83.4	88.0	-93.0	-98.1[a]	-103.4	-108.1	-111.8	P, Pt	1.80

[a] *Highest intensity peak*

[b] *Silica polymorphs **[17]**: quartz (-108); coesite (–108 ,-113.9); cristobalite (-108.5) tridymite (-109 to -114)*

[c] *S = sodalite, C= Na-chabazite, Y = zeolite Y, P = zeolite P and P_t = phillipsite*

[d] *Calculated from the Engelhard equation **[17]***

[e] signal associate to mullite present in the starting fly ash ***[8,11,16]***

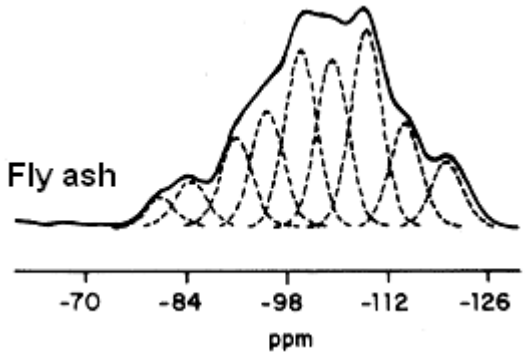

Figure 1. ^{29}Si NMR-MAS spectrum of the initial fly ash

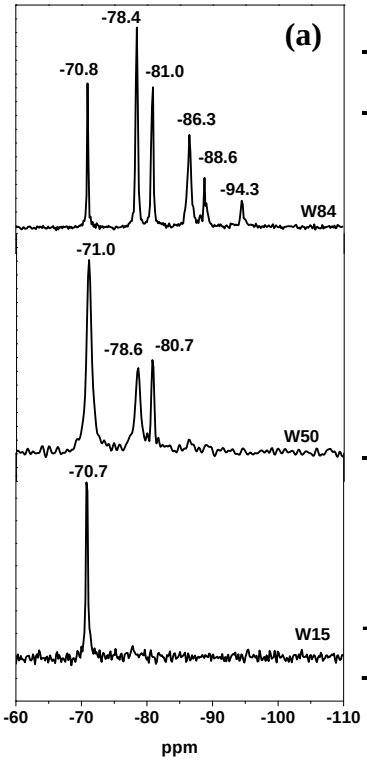

(b)

Solution	-δ ppm	Area (%)	Q^n site	Structure	Silicate species
W84	**-70.8**	**14.5**	**Q^0**		**Monomer**
	-78.4	**(23.7)***	**Q^1**		**Dimer**
	-78.4	**(23.7)***	**Q^1**		**Linear Trimer**
	-88.6	**8.5**	**Q^2**		
	-81.0	**24.6**	**C^2_{cyc}**		**Cyclic Trimer**
	-86.3	**24.3**	**Q^2_{cyc}**		**Bridged cyclic tetramer**
	-94.3	**4.4**	**Q^3_{cyc}**		
W50	**-71.0**	**59.2**	**Q^0**		**Monomer**
	-78.6	**25.3**	**Q^1**		**Dimer**
	-81.43	**15.5**	**C^2_{cyc}**		**Cyclic Trimer**
W15	**-70.7**	**100**	**Q^0**		**Monomer**

*** Overlapping signal**

Figure 2. (a) ^{29}Si MAS-NMR spectra of the alkaline solutions used; (b) ^{29}Si chemical shift, δ, of the silicate anion in silicate solutions, identified in accordance with the literature **[17,18]**.

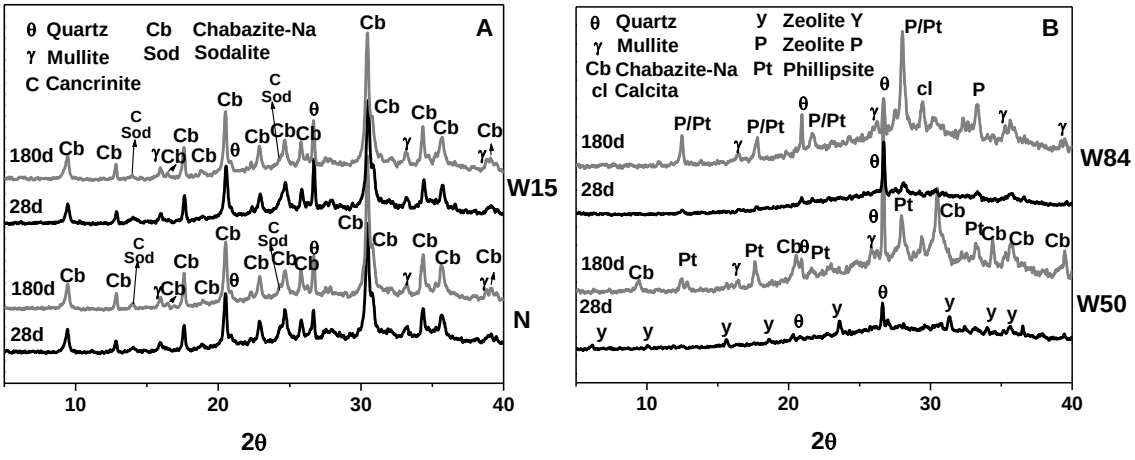

Figure 3. X-ray powder diffraction patterns of ash activated with different alkaline solutions (28 and 180 days).

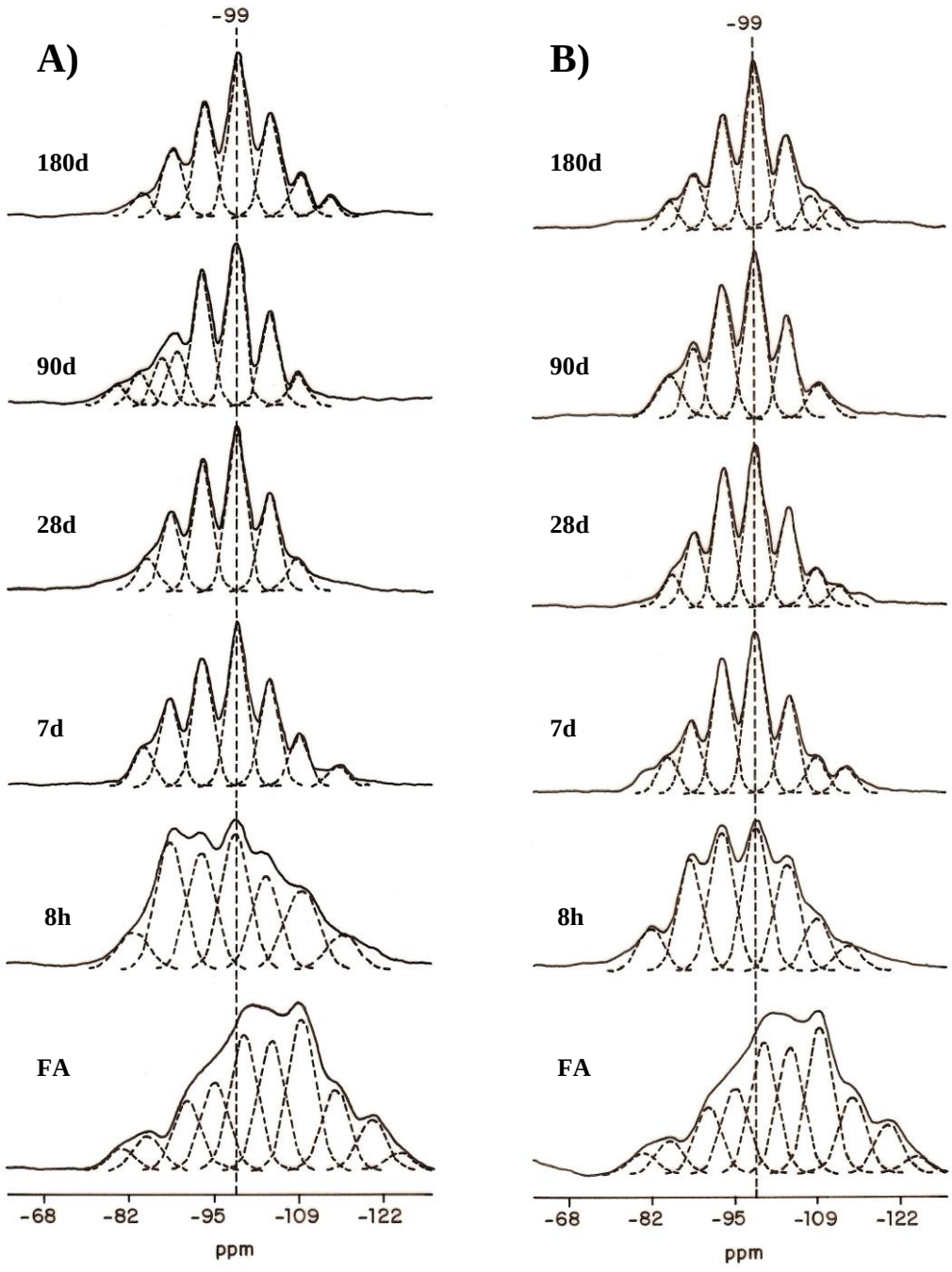

Figure 4. ^{29}Si MAS NMR-MAS spectra of AAFA pastes activated with solution (a) N and (b) W15;

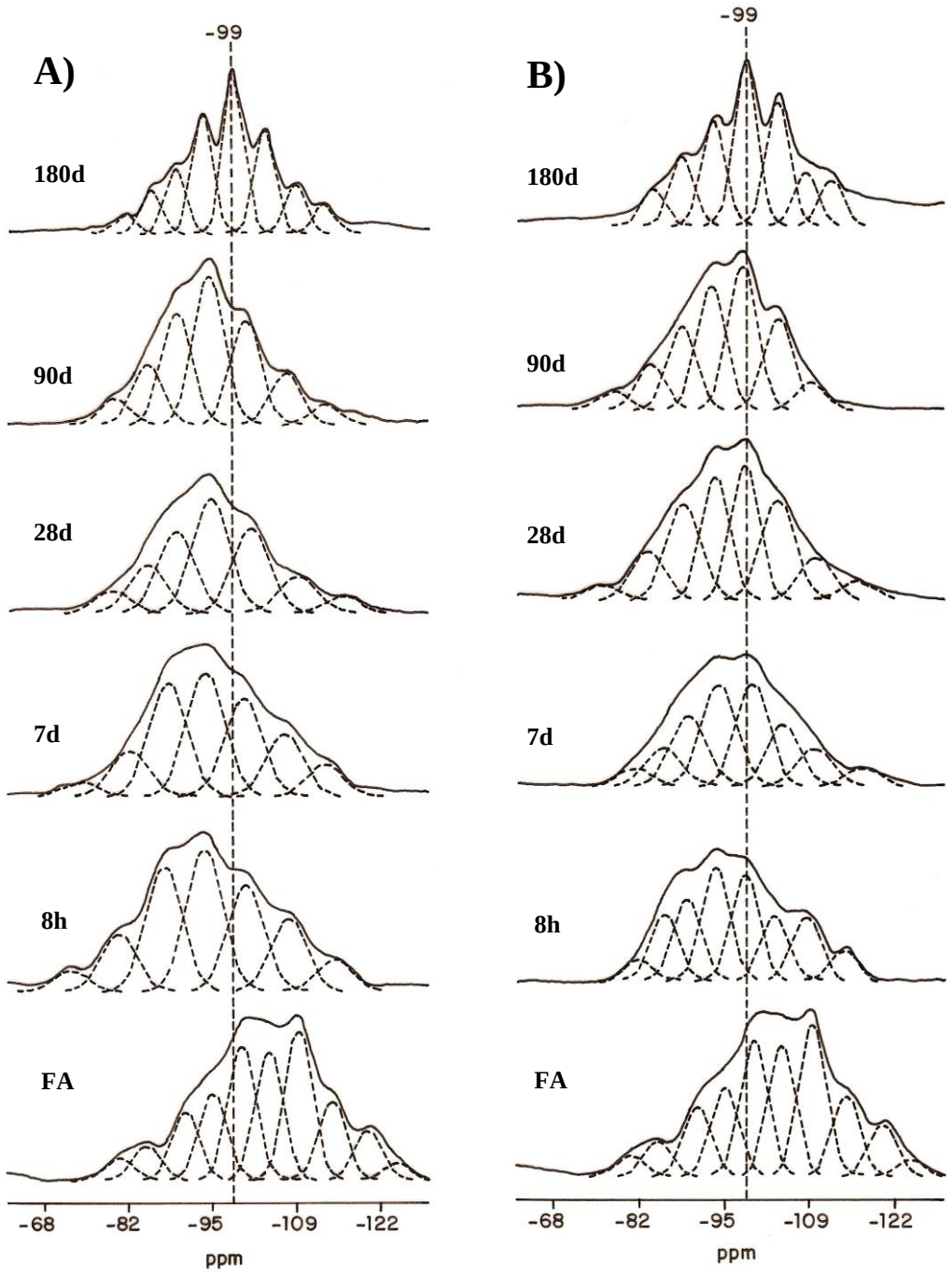

Figure 5. ^{29}Si MAS NMR-MAS spectra of AAFA pastes activated with solution (a) W50 and (b) W84

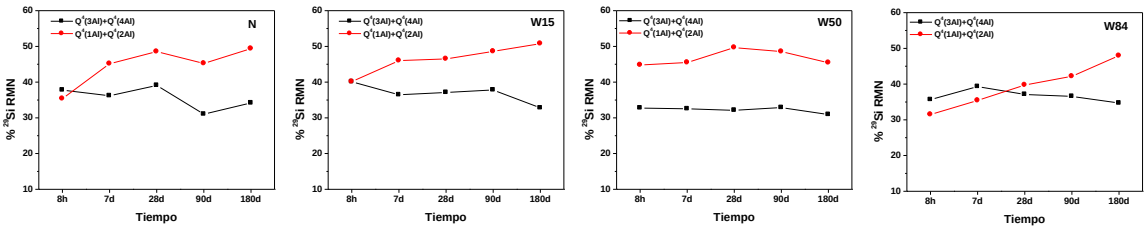

Figure 6. Variation in aluminium-rich ($Q^4(4Al)+Q^4(3Al)$) and silicon-rich ($Q^4(2Al)+Q^4(1Al)$) environments with reaction time, deduced from the ^{29}Si MAS NMR spectra for alkali-activated fly ash materials

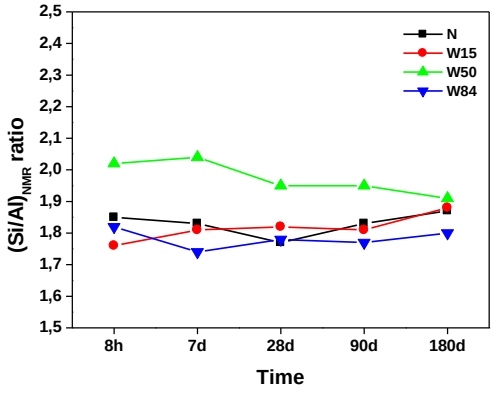

Figure. 7. Si/Al ratios versus time in fly ash activated with solutions: N; W15; W50 and W84

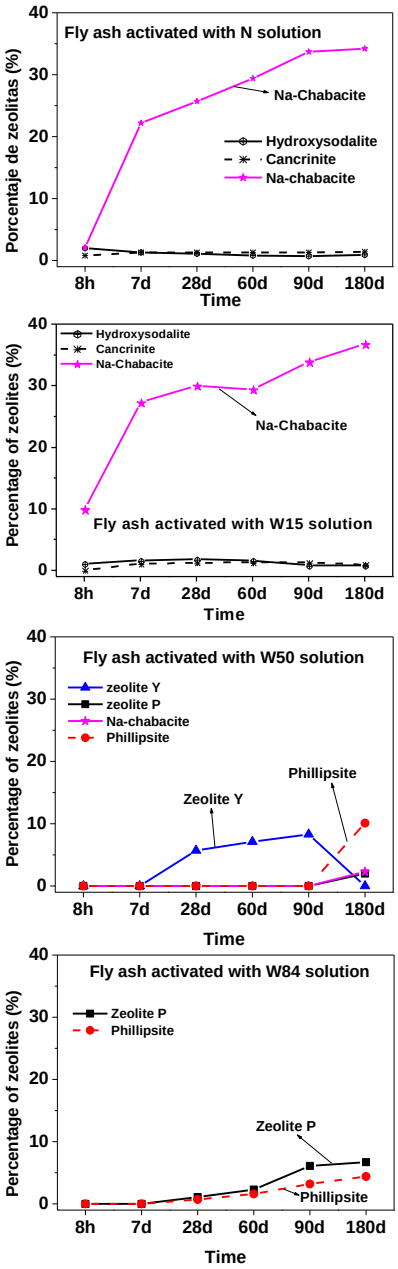

Figure 8. Percentage of zeolite phases in the matrices studied vs curing time (data obtained with XRD, using Rietveld methodology **[22]**).